scientific reports

Check for updates

OPEN

L-ascorbate prevents non-alcoholic steatohepatitis-based hepatocarcinogenesis in *Sod1/Prdx4* double-knockout mice

Tsukasa Osaki[1]✉, Takujiro Homma[1,6], Yuki Maeda[2], Ken-ichi Yamada[3], Chikako Yokoyama[4], Shinya Toyokuni[2,5] & Junichi Fujii[1]

Superoxide dismutase 1 (*Sod1*) and peroxiredoxin 4 (*Prdx4*) double knockout (DKO) causes symptoms similar to non-alcoholic steatohepatitis (NASH) even at younger ages. This study revealed that DKO mice exhibited high mortality, and surviving DKO mice developed hepatocellular carcinoma within the first year of life. Administration of physiological doses of L-ascorbate (Asc; 1.5 mg/mL) in drinking water reduced mortality and effectively prevented tumor development. Oxidative stress due to SOD1 deficiency and endoplasmic reticulum stress due to PRDX4 deficiency may promote NASH, ultimately leading to hepatocarcinogenesis. Analyses of liver tissues from 8-month-old DKO mice revealed that Asc supplementation robustly suppressed upregulation of amino acid metabolic pathways observed in DKO mice. These findings suggest that upregulation of amino acid metabolic pathways may be important for the hepatocarcinogenesis. An iron-regulatory protein and aconitase activity were decreased in DKO mice regardless of Asc status. Furthermore, precancerous lesions were more reactive to a ferroptosis-specific antibody than tumor lesions. These results suggest that Asc supplementation and aberrant iron metabolism selectively induce the death of cells that lead to tumorigenic proliferation at the precancerous stage. Adequate intake of Asc in daily life may improve the tumorigenic process promoted by hepatic steatosis due to oxidative insult.

Keywords Non-alcoholic steatohepatitis, Hepatic tumor, Endoplasmic reticulum stress, Oxidative stress, Iron regulatory protein

Abbreviations

NAFLD	Non-alcoholic fatty liver disease
NASH	Non-alcoholic steatohepatitis
ROS	Reactive oxygen species
SOD	Superoxide dismutase
KO	Knockout
ER	Endoplasmic reticulum
PRDX	Peroxiredoxin
Asc	Ascorbate
WT	Wild-type
DKO	Double knockout
GO	Gene ontology
PCA	Principal component analysis

[1]Department of Biochemistry and Molecular Biology, Graduate School of Medical Sciences, Yamagata University, 2-2-2 Iidanishi, Yamagata 990-9585, Japan. [2]Department of Pathology and Biological Responses, Nagoya University Graduate School of Medicine, 65 Tsurumai-Cho, Showa-Ku, Nagoya 466-8550, Japan. [3]Faculty of Pharmaceutical Sciences, Physical Chemistry for Life Science Laboratory, Kyushu University, 3-1-1 Maidashi Higashi-Ku, Fukuoka 812-8582, Japan. [4]Department of Chemistry and Bioengineering, Graduate School of Engineering, Osaka Metropolitan University, 3-3-138, Sugimoto, Sumiyoshi-Ku, Osaka-Shi 558-8585, Japan. [5]Center for Low-Temperature Plasma Sciences, Nagoya University, Furo-Cho, Chikusa-Ku, Nagoya 464-8603, Japan. [6]Department of Pharmacology, Osaka Metropolitan University Graduate School of Medicine, 1-4-3 Asahi-Machi, Abeno-Ku, Osaka-Shi 545-8585, Japan. ✉email: tosaki@med.id.yamagata-u.ac.jp

TCA	Tricarboxylic acid cycle
NRF2	Nuclear factor erythroid 2-related factor 2
ACO1	Aconitase 1
ACO2	Aconitase 2
RT	Reverse transcription
ANOVA	Analysis of variance

Non-alcoholic fatty liver disease (NAFLD) is defined as fat accumulation exceeding 5% of hepatocyte volume in the absence of a history of alcohol overconsumption. Such a condition has been known to advance to non-alcoholic steatohepatitis (NASH) in 2–5% of the general population[1,2]. Although the mechanism by which NAFLD progresses to NASH has not yet been fully elucidated, recent reports suggest that iron overload is involved in the progression of NAFLD[3]. It is thought that ferroptosis caused by iron overload leads to liver damage and inflammatory infiltration. Without appropriate treatment, NASH could progress to a hepatic tumorigenesis through cirrhosis, and inflammation plays a primary role in this process[4,5]. Reactive oxygen species (ROS) are generally elevated under inflammation, and oxidative stress is believed to be a potential underlying mechanism in the tumorigenesis processes[6,7]. However, due to the lack of suitable animal models reproducing the pathogenic processes, the underlying mechanisms in the progression of this disease remain ambiguous.

Superoxide is a primary oxygen radical generated by various oxygen-consuming reactions, but in the presence of free iron, it could be converted to more harmful ROS such as hydroxyl radicals. Superoxide dismutase (SOD) plays a pivotal role in preventing oxidative damage and associated diseases caused by ROS[8]. Knockout (KO) of *Sod1*, which encodes a cytosolic Cu- and Zn-containing SOD, increases susceptibility to liver steatosis in mice[9]. This is associated with impaired lipoprotein secretion due to endoplasmic reticulum (ER) stress. Although a subset of aged *Sod1*-KO mice spontaneously develops hepatic tumors[10], co-deficiency of the tumor suppressor gene Ataxia-telangiectasia mutated, which plays a role in DNA repair, and treatment with antioxidants such as α-tocopherol do not affects the survival or tumorigenesis of *Sod1*-KO mice[11]. Mice with both *Sod1* gene deletion and the obese diabetic mutation of the leptin receptor do not develop NASH even when fed a high-fat diet for a long period of time, despite an extraordinary accumulation of visceral fat and massive deposits of lipid droplets in the liver. Thus, the combination of oxidative stress caused by SOD1 deficiency and DNA damage or high-fat loading does not promote NASH or hepatic tumor development of either in mice.

ER stress is considered another underlying promoter of NASH and hepatic tumorigenesis[12,13]. Conventional cultivation of primary hepatocytes isolated from *Sod1*-KO mice stimulates lipogenesis in part through the aberrant activation of sterol regulatory element binding transcription proteins. These proteins could be activated by ER stress as well as by sterol insufficiency[14]. Peroxiredoxin (PRDX) 4 is an ER-resident thiol oxidase that utilizes the oxidizing the power of hydrogen peroxide to participate in the oxidative folding of nascent proteins in the secretory pathway[15,16]. While deficiency of either PRDX4 or ER oxidoreductin 1[17] alone results in subtle phenotypic abnormalities, deficiency of both of these genes leads to atypical scurvy in mice due to ascorbate (Asc) consumption and aberrant collagen synthesis[18]. Consistent with these observations, transgenic overexpression of *Prdx4* mitigates NASH and/or type 2 diabetes induced by the feeding of a high-fructose diet[19]. Furthermore, the administration of hepatocarcinogen *N*-nitrosodiethylamine increases the incidence of tumor development in *Prdx4*-KO mice compared with that in wild-type (WT) mice, but the transgenic overexpression of *Prdx4* consistently decreases the rate[20]. Thus, PRDX4 plays a role in maintaining liver homeostasis through normalization of the ER function.

Mice with a double knockout of *Sod1* and *Prdx4*, which are referred to as DKO mice in this communication, show NASH-like symptoms that are not evident in either *Sod1*-KO or *Prdx4*-KO mice[21]. In the current study, we found that DKO mice raised under conditions of conventional breeding for 12 months developed hepatic tumors and that supplementation of Asc in drinking water markedly reduced both mortality and tumor incidence. Since tumorigenic changes progress before tumor becomes detectable, it was thought that understanding the differences in proteins and metabolites before 12 months would help elucidate the progression from NASH to liver tumor. We conducted an analysis at the 8-month stage, when precancerous lesions were thought to be present. Although Asc is generally considered an antioxidant, it has a pro-oxidant effect that couples with reactions that reduce metal ions such as Fe^{3+} to generate ROS such as hydroxyl radicals[22]. Since iron metabolism is prone to impairment in DKO mice, it is thought that Asc in association with free iron to eliminate cells that are destined for tumorigenic transformation at the precancerous stage by ferroptosis.

Results

Hepatic tumor development in *Sod1*/*Prdx4* DKO mice is suppressed by Asc supplementation

We previously reported that DKO mice develop NASH-related symptoms even at a young age[21]. In the present study, we observed four genotypes of male mice — WT, *Sod1*-KO, *Prdx4*-KO, and DKO — over the first year of life. As *Sod1*-KO mice have been reported to exhibit low plasma Asc levels[23], and Asc is a candidate tumor suppressor due to its ability to counteract oxidative stress, we also included additional groups of *Sod1*-KO and DKO mice supplemented with Asc (1.5 mg/mL in drinking water).

Although plasma Asc levels in *Prdx4*-KO mice (47.9 ± 4.9 μM, $n = 4$) were comparable to those in WT mice, DKO mice showed significantly lower plasma Asc levels than WT and *Prdx4*-KO mice. Supplementation restored Asc levels in DKO mice to those of WT mice (Fig. 1A). DKO mice exhibited a high mortality rate, which was ameliorated by Asc supplementation (Fig. 1B). After one year, autopsy revealed numerous hepatic tumor nodules in DKO mice (Fig. 1C). Among 10 *Sod1*-KO mice, 3 developed multiple tumors ≥ 5 mm, 2 developed multiple tumors of 1–2 mm, and 5 remained tumor-free ($P = 0.0935$). Among 7 DKO mice, 3 developed multiple tumors ≥ 5 mm, 3 developed multiple tumors of 3–5 mm, and 1 developed tumors of 1–2 mm ($P = 0.0007$).

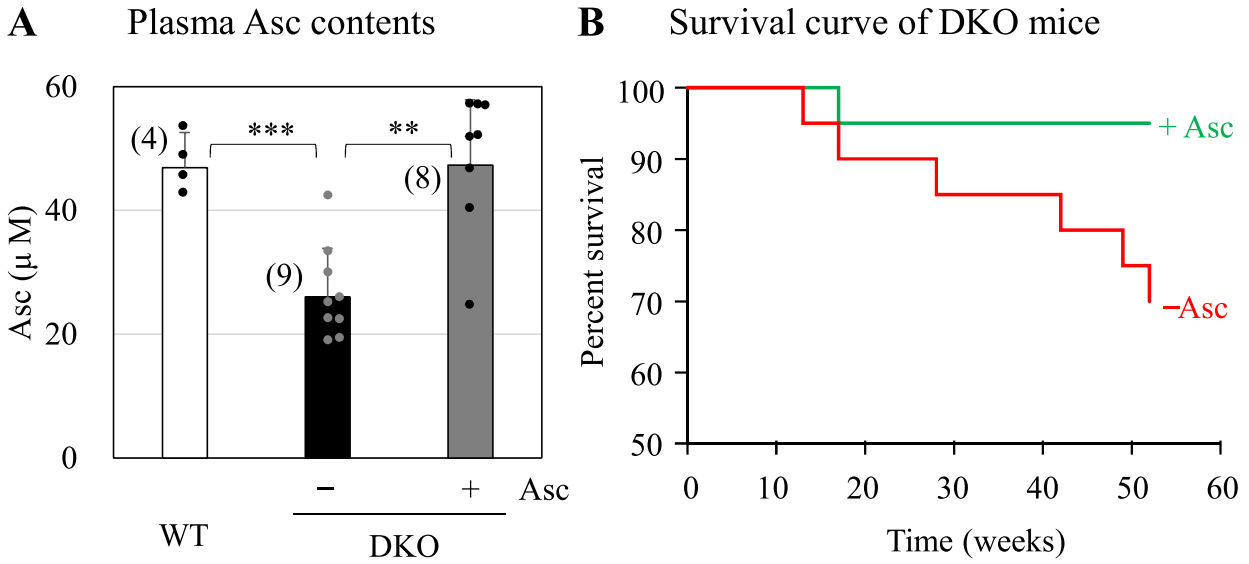

C

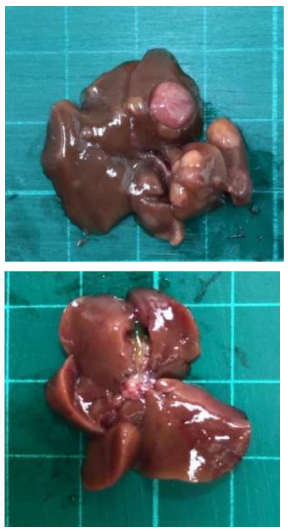

Asc	Tumor bearing/total mice (12 Mo)			
	WT	*Prdx4*-KO	*Sod1*-KO	DKO
−	1/8	2 /10	5/10	7 /7
+	−	−	1/10	2 /9

Fig. 1. Asc alleviated tumor development and mortality in DKO mice. (**A**) Plasma Asc levels were measured using a fluorescent probe. The number of animals is indicated in parentheses. Statistical analysis was performed using one-way ANOVA followed by the Tukey–Kramer test. $^{**}P<0.01$; $^{***}P<0.001$. (**B**) Male DKO mice with (1.5 mg/mL in drinking water) or without Asc supplementation were observed for up to one year ($n=20$ per group). Survival curves were compared using the log-rank test ($P=0.0425$). (**C**) Representative livers from DKO mice at 12 months (12 Mo). After one year, mice were euthanized and the numbers of visible hepatic tumors were determined. The incidence of tumor-bearing mice was compared among the four genetic groups. Chi-square analysis revealed *P*-values of 0.6714, 0.0935, and 0.0007 for *Prdx4*-KO, *Sod1*-KO, and DKO groups, respectively, compared with WT. Asc was supplemented in *Sod1*-KO and DKO groups. Chi-square analysis showed a significant difference in tumor incidence between groups with and without Asc ($P=0.0510$ for *Sod1*KO mice and $P=0.0019$ for DKO mice).

Thus, although *Sod1*-KO mice showed a modest increase in tumor incidence, DKO mice exhibited both a higher frequency and larger tumor burden.

By contrast, Asc supplementation markedly suppressed tumor development in both *Sod1*-KO ($P=0.0510$) and DKO mice ($P=0.0019$). Among 9 DKO mice receiving Asc, only 1 developed a single tumor of 3–5 mm, 1 developed a single tumor of 1–2 mm, and 7 remained tumor-free. Based on these findings, subsequent experiments focused on DKO mice with and without Asc supplementation, with WT mice serving as controls (Supplementary Fig. 1). Because tumors were rarely detectable at 8 months of age, the premature deaths observed in DKO mice at young adult stages were unlikely attributable to tumor development.

Excessive inflammation in DKO mice is independent of macrophage dysfunction and minimally affected by ascorbic acid

Because innate immune cells play central roles in inflammation and are associated with tumor development [6,7], we examined blood cells from WT, DKO and DKO mice supplemented with Asc at 4 and 8 months of age (Supplementary Fig. 2). The reduced body weight and lower red blood cell counts observed in DKO mice are likely phenotypic traits inherent to SOD1 deficiency[24]. White blood cell counts, particularly lymphocytes and granulocytes, were elevated in 4-month-old DKO mice, consistent with the inflammatory conditions characteristic of NASH, and Asc supplementation appeared to have minimal effect. Unexpectedly, the difference in lymphocyte counts between WT and DKO mice was smaller at 8 months of age. In addition, plasma levels of inflammatory cytokines (TNFα, IL-1β, and IFN-γ) did not differ significantly among the three groups at either 4 or 8 months (Supplementary Fig. 3). Based on these findings, we hypothesized that DKO mice with severe inflammatory disorders may die before developing tumors, whereas those with relatively mild NASH phenotypes survive longer and eventually develop hepatic tumors.

Because macrophages are key mediators of inflammatory processes[4,5], we next isolated peritoneal macrophages from 4-month-old mice, stimulated them with LPS in vitro, and assessed the expression of several activation markers. However, indicators of macrophage activation, including nitric oxide production, CD80, and CD11b, did not differ among the groups (Supplementary Fig. 4). These results suggest that aberrant macrophage function is unlikely to underlie the excessive inflammatory responses observed in DKO mice.

Asc suppresses hepatocyte atypia but not characteristic ferroptosis in DKO mice

Next, we performed pathological analyses of the livers from 8-month-old DKO mice with or without Asc supplementation and compared them with those of WT mice. In 12-month-old DKO mice, tumors had developed in the group without Asc supplementation; however, histological examination with hematoxylin and eosin staining at 8 months revealed no obvious fibrosis—considered a precursor to tumor development—in any of the DKO groups (Fig. 2A). Compared with WT mice, livers of DKO mice displayed precancerous changes, including hepatocyte atypia, accompanied by lymphocytic infiltration and regenerative alterations. Asc supplementation suppressed hepatocyte atypia, including nuclear enlargement and irregular size.

Ferroptosis, an iron-dependent, non-apoptotic form of cell death, is thought to contribute to NASH[3,25]. Therefore, we examined ferroptotic cell distribution using FerAb, which specifically recognizes ferroptotic cells[26]. FerAb staining revealed a marked increase in ferroptotic cells in the DKO group compared with WT mice, whereas Asc supplementation had little effect. In 12-month-old DKO mice, atypical cells with enlarged nuclei were predominantly stained in noncancerous regions, but not in cancer cells (Fig. 2B), suggesting that cells in precancerous lesions are more susceptible to ferroptosis than cancer cells. To further assess ferroptosis-related proteins, we analyzed GPX4 expression by immunoblotting and found no significant differences among groups (Supplementary Fig. 5).

Proteomic analysis of DKO mouse livers reveals Asc-sensitive alterations in amino acid metabolism associated with tumorigenesis

Due to the high frequency of hepatic tumor development following NASH, DKO mice were considered to be a useful model for analyzing the tumorigenesis process. Therefore, we performed proteomic analysis using the livers of 8-month-old WT and DKO mice, which had not yet formed obvious tumor nodules, and compared the results. Volcano plots show that many proteins were increased in the livers of DKO mice compared with WT mice (Fig. 3A, Supplementary Table 1). Of these proteins, eight proteins, including quinone oxidoreductase (CRYZ) with quinone reduction activity, and homogentisate 1, 2-dioxygenase (HGD) and mitochondrial 2-amino-3-ketobutyrate coenzyme A ligase (GCAT), involved in amino acid metabolism, were significantly decreased by Asc supplementation (Fig. 3 B). On the other hand, of the 131 proteins that were significantly increased in DKO mice compared with WT mice, and of the 8 proteins that significantly decreased, the significant differences were no longer observed in Asc-supplemented DKO mice compared with WT mice (Supplementary Fig. 6). Gene ontology (GO) analysis showed that proteins that were significantly increased only in DKO mice without Asc supplementation were largely associated with amino acid metabolism, while decreased proteins were not related to each other. Supplementation with Asc significantly suppressed tumor formation and increased proteins related to amino acid metabolism, suggesting that alteration of amino acid metabolism is involved in the tumorigenesis process.

Metabolomic profiling of DKO mouse livers reveals alterations in glycometabolism and amino acid metabolism

Given the involvement of altered metabolic pathways in tumorigenesis, we performed metabolite analysis of liver extracts (Supplementary Table 2). Volcano plots demonstrated that many metabolites were significantly increased or decreased in DKO mice compared with WT mice, and that for some metabolites, the differences observed between WT and DKO mice were no longer statistically significant when comparing WT with Asc-supplemented DKO mice (Fig. 4A). A Venn diagram further showed that half of the 18 metabolites significantly increased in DKO mice and 8 of the 34 significantly decreased metabolites lost statistical significance in the comparison between WT and Asc-supplemented DKO mice, although their levels did not necessarily return to those of WT mice (Fig. 4B).

A heat map indicated alterations in glycometabolism, including glycolysis and the pentose phosphate pathway (Fig. 4C), as well as in amino acid metabolism (Fig. 4D). Principal component analysis (PCA) revealed that the three groups (WT, DKO, and DKO supplemented with Asc) could be distinguished based on glycometatolic products (Fig. 4C). For amino acid metabolism, PCA clearly separated WT from DKO and Asc-supplemented DKO, but did not distinguish between DKO and Asc-supplemented DKO (Fig. 4D). The nanoflow liquid

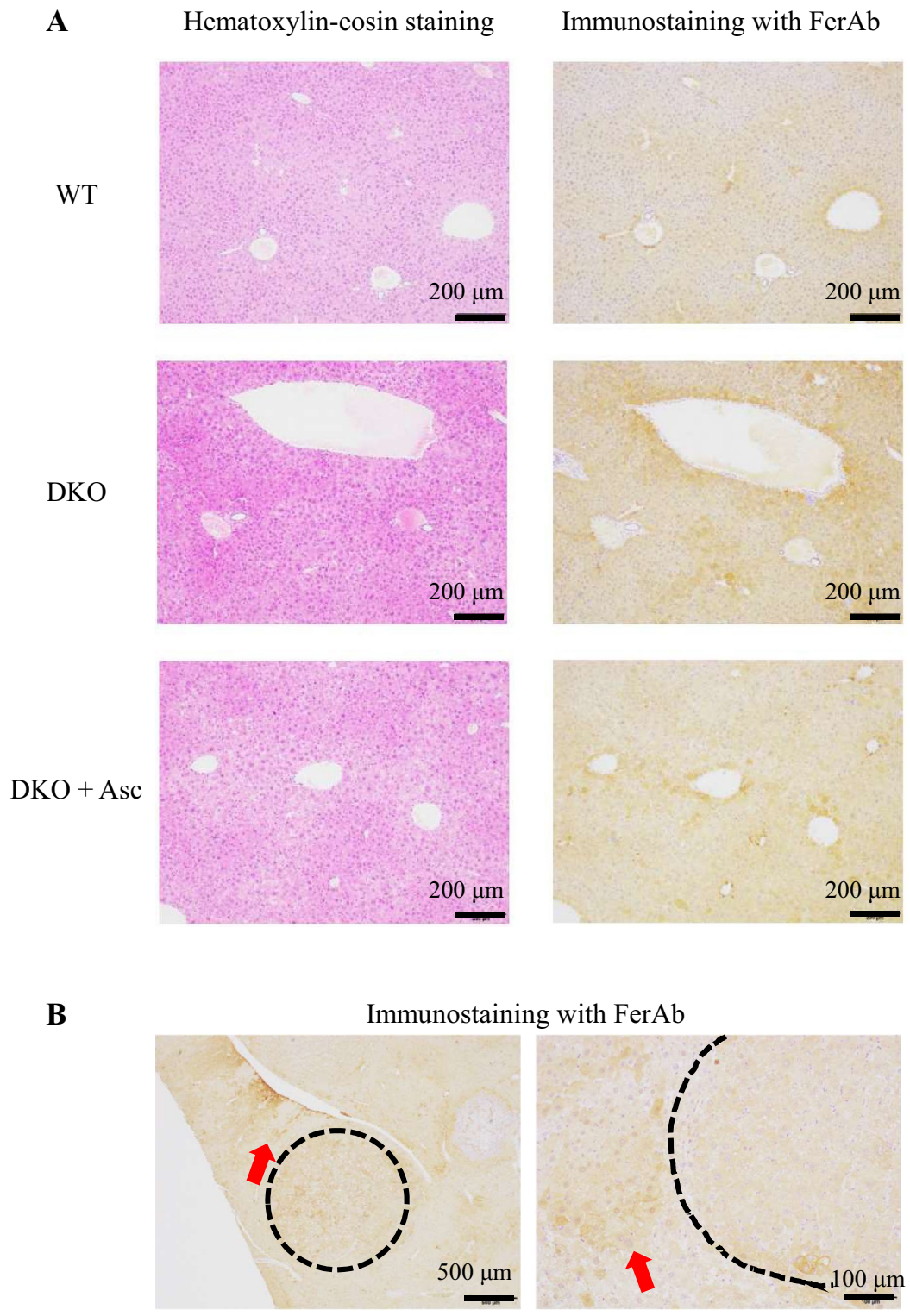

Fig. 2. Histological analyses of mice livers. (**A**) Liver Sects. (5 μm in thickness) of WT, DKO, and DKO mice supplemented with Asc (DKO + Asc) at 8 months of age were subjected to hematoxylin–eosin staining and immunohistochemical staining using FerAb. Number of animals is 4 each. (**B**) Cancerous and precancerous areas in the liver of a 12-month-old mouse are indicated by the dotted lines and red arrows, respectively. The right panel is an enlargement of the left panel.

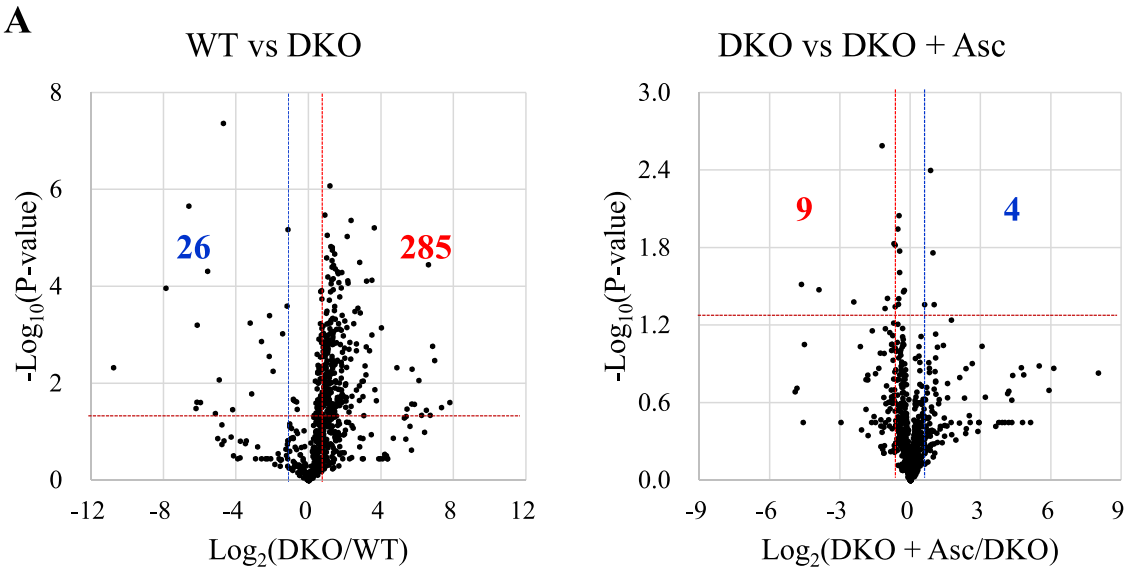

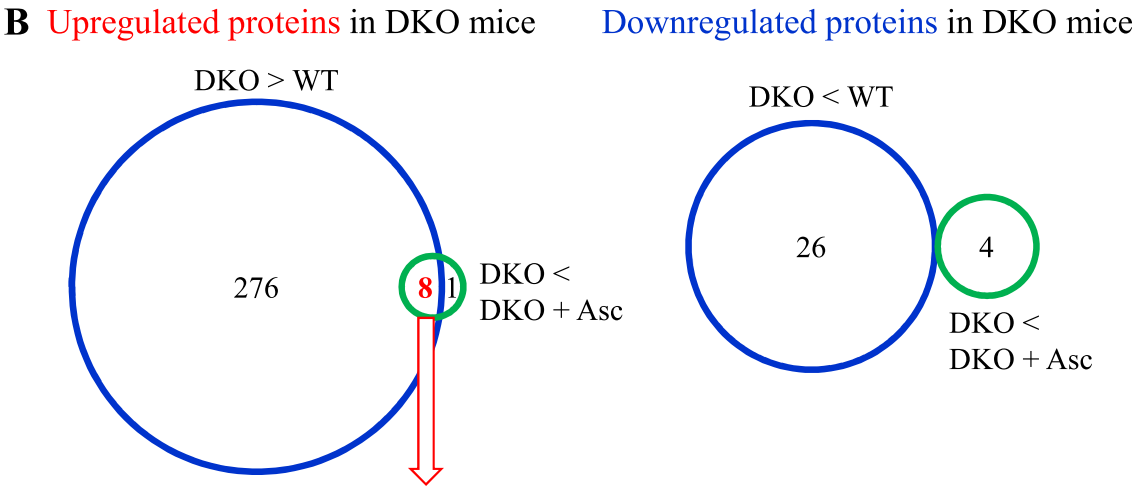

CRYZ, Quinone oxidoreductase
HGD, Homogentisate 1,2-dioxygenase
PSMA7, Proteasome subunit alpha type-7
GCAT, 2-amino-3-ketobutyrate coenzyme A ligase, mitochondrial
PABPC1, Polyadenylate-binding protein 1
PZP, Pregnancy zone protein
PYGL, Glycogen phosphorylase, liver form
DLST, Dihydrolipoyllysine-residue succinyltransferase component of 2-oxoglutarate dehydrogenase complex, mitochondrial

Fig. 3. Proteomic analyses of the livers from DKO mice compared with WT mice or DKO mice with Asc supplementation. Proteins were extracted from the liver tissues of mice at 8 months of age and subjected to trypsinization followed by proteomic analyses via nanoflow liquid chromatography tandem mass spectrometry. Statistical analyses were performed using a Student's *t*-test for comparisons of two groups. (**A**) The volcano plot of the data compares the proteins in DKO mice *vs.* those in WT mice (left panel) and proteins in DKO mice supplemented with Asc (DKO + Asc) *vs.* proteins in DKO mice (right panel). The blue and red lines indicate levels in DKO mice that were 0.67- and 1.5-fold higher than in WT mice, and 0.67- and 1.5-fold higher than in DKO mice supplemented with Asc, respectively. (**B**) The Venn diagram indicates the numbers of proteins that were either upregulated (left: ratio > 1.5; *P*-value < 0.05) or downregulated (right: ratio < 0.67; *P*-value < 0.05) between two mice groups. Number of animals is 3 each.

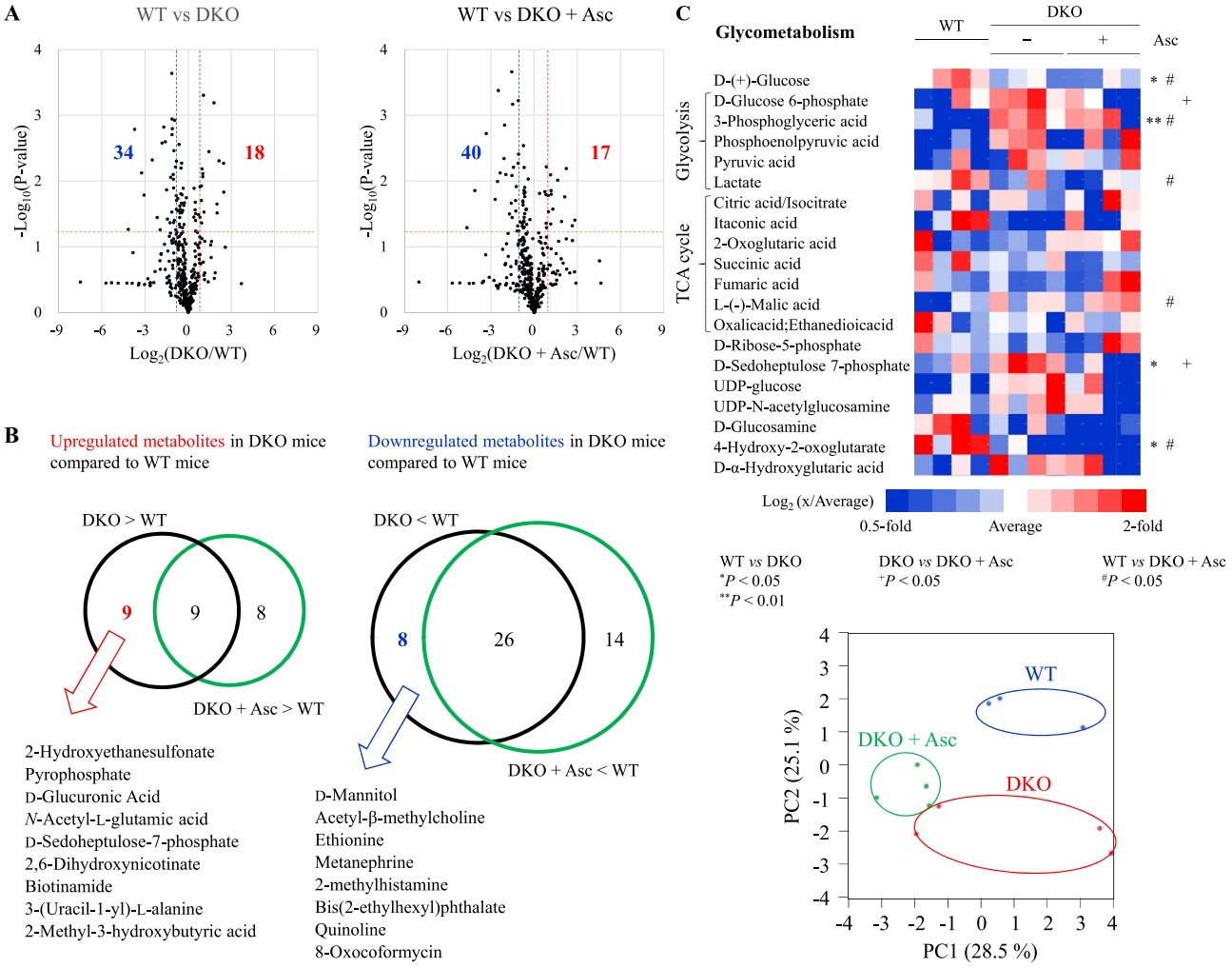

Fig. 4. Comparison of metabolites among three groups of mice at 8 months of age. Liver soluble metabolites were analyzed by liquid chromatography-tandem mass spectrometry. Statistical analyses were performed using Student's *t*-test. (**A**) Volcano plots comparing DKO *vs.* WT mice (left) and DKO + Asc *vs.* WT mice (right). Blue and red lines indicate 0.67- and 1.5-fold thresholds, respectively. (**B**) Venn diagrams showing upregulated (fold change > 1.5, $P < 0.05$) and downregulated (fold change < 0.67, $P < 0.05$) metabolites between groups. Metabolites altered in DKO mice but normalized by Asc supplementation are listed. $n = 3$ per group. (**C**, **D**) Heatmap and PCA score plots of metabolites involved in glycometabolism (C) and amino acid metabolism (D). (E) Representative metabolites of central metabolism mapped onto glycolysis (linked to the pentose phosphate pathway), the TCA cycle, and the urea cycle.

chromatography tandem mass spectrometry system used in this study could not discriminate between several metabolites with identical molecular masses, such as citrate/isocitrate and glucose-6-phosphate/glucose-1-phosphate/fructose-6-phosphate.

Notably, elevation of sedoheptulose-7-phosphate, an intermediate of the pentose phosphate pathway, suggests increased carbon flux into this pathway (Fig. 4E). Changes in several amino acid levels further imply enhanced amino acid catabolism. While levels of tricarboxylic acid (TCA) cycle intermediates were similar between WT and DKO mice, some of these compounds were increased in Asc-supplemented DKO mice (Fig. 4C).

Antioxidant response and protein turnover in the livers of DKO mice

Many gene products involved in antioxidation and detoxification reactions were elevated in the livers of DKO mice (Fig. 5A), and we considered this upregulation to be a compensatory response to oxidative stress due to SOD1 deficiency. Nuclear factor erythroid 2-related factor 2 (NRF2) is the master regulator of the antioxidant system, and it is stabilized in response to oxidative insult and is translocated to the nucleus to induce multiple genes, including those acting in antioxidation[27]. To examine the participation of NRF2 in the expressions of antioxidant genes, we isolated nuclei from the livers of 8-month-old DKO mice and examined the NRF2 content via immunoblot analysis using an anti-NRF2 antibody. Although there were large individual differences, nuclear-translocated NRF2 protein tended to be increased in the liver of DKO mice, which was not affected by Asc supplementation (Fig. 5B). This trend was also confirmed via quantitative PCR. Since there was also a large

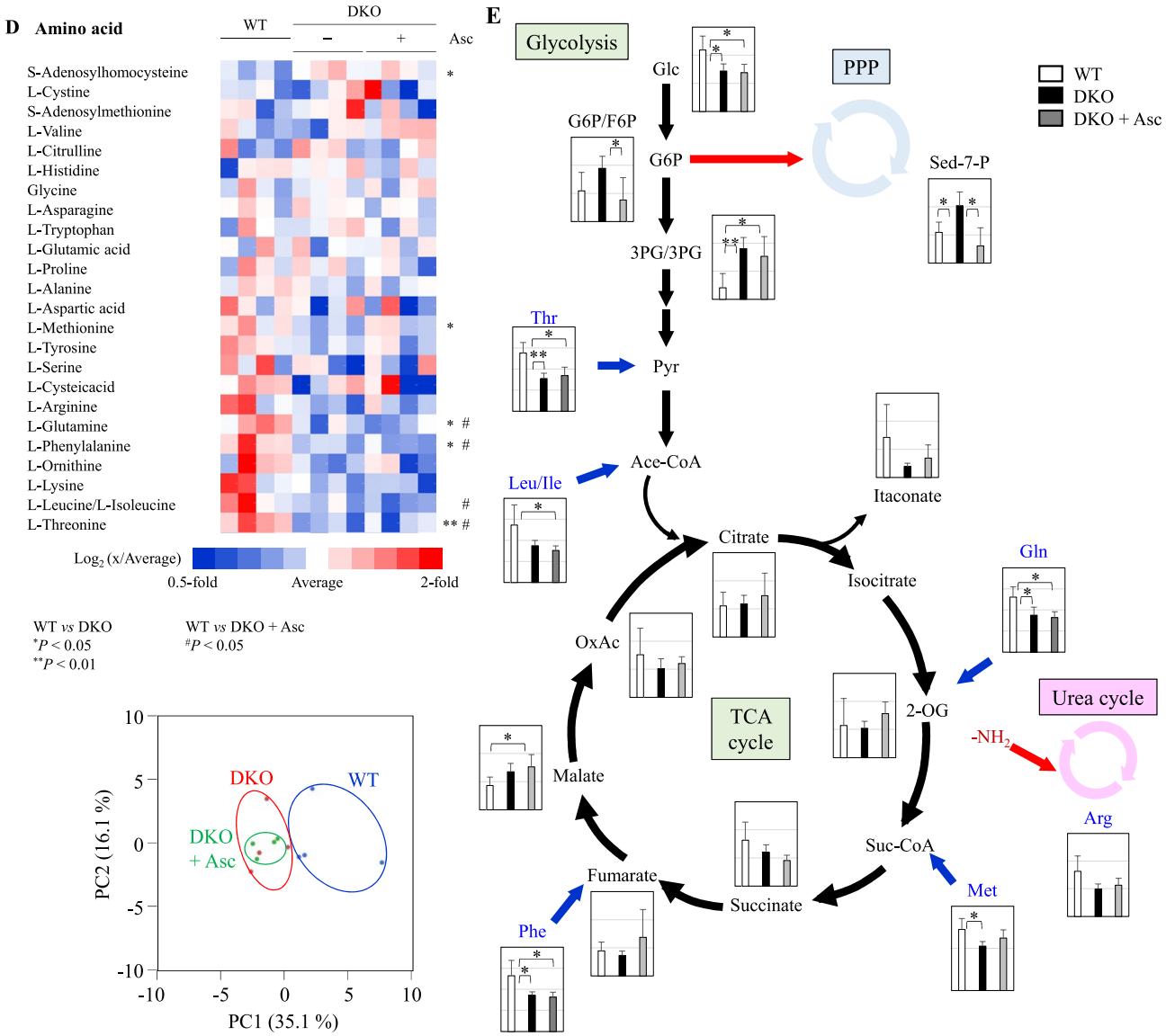

Fig. 4. (continued)

individual difference in body sizes at 8 months of age, we examined the relationship between body weight and nuclear NRF2 content and discovered an inverse correlation (Fig. 5C). Nrf2 activation was more pronounced in low-weight DKO mice, likely due to severe liver damage caused by stress. This trend was not changed by Asc supplementation, suggesting that it is insufficient to inhibit the promotion to the precancerous stage. Therefore, it appears that subsequent processes must be suppressed via supplementation with Asc to inhibit tumor progression. Because elevated oxidation is one of the mechanisms for altered gene expression, we tried to evaluate the state of protein oxidation via detection of carbonyl proteins. However, it was surprising that the levels of carbonyl proteins in the liver of DKO mice were lower compared with WT mice, regardless of Asc supplementation (Supplementary Fig. 7). Because polyubiquitination of oxidatively damaged and aged proteins accelerates their degradation by the proteasome[28,29], we evaluated the levels of polyubiquitinated proteins via immunoblot analysis using an anti-ubiquitin antibody and found subtle elevations in the levels in DKO mice (Supplementary Fig. 8). Taken together, these data suggest that polyubiquitination occurs preferentially on oxidatively damaged proteins in the liver of DKO mice, stimulating their degradation by proteasomes, although the proteolytic capacity of the proteasomes was unchanged, as judged by the levels of the catalytic β-subunits β1, β2 and β5 (Supplementary Fig. 9).

Dysregulation of iron metabolism and decreased aconitase activity in DKO mice

Since the combined presence of free iron and peroxides induces ferroptosis — an iron-dependent, non-apoptotic form of cell death — through the generation of hydroxyl radicals[30,31], we examined the levels of cytosolic aconitase 1 (ACO1), which functions as an iron regulatory element-binding protein in iron homeostasis[32], together with mitochondrial aconitase 2 (ACO2), a key enzyme in the TCA cycle. Immunoblot analysis revealed that hepatic

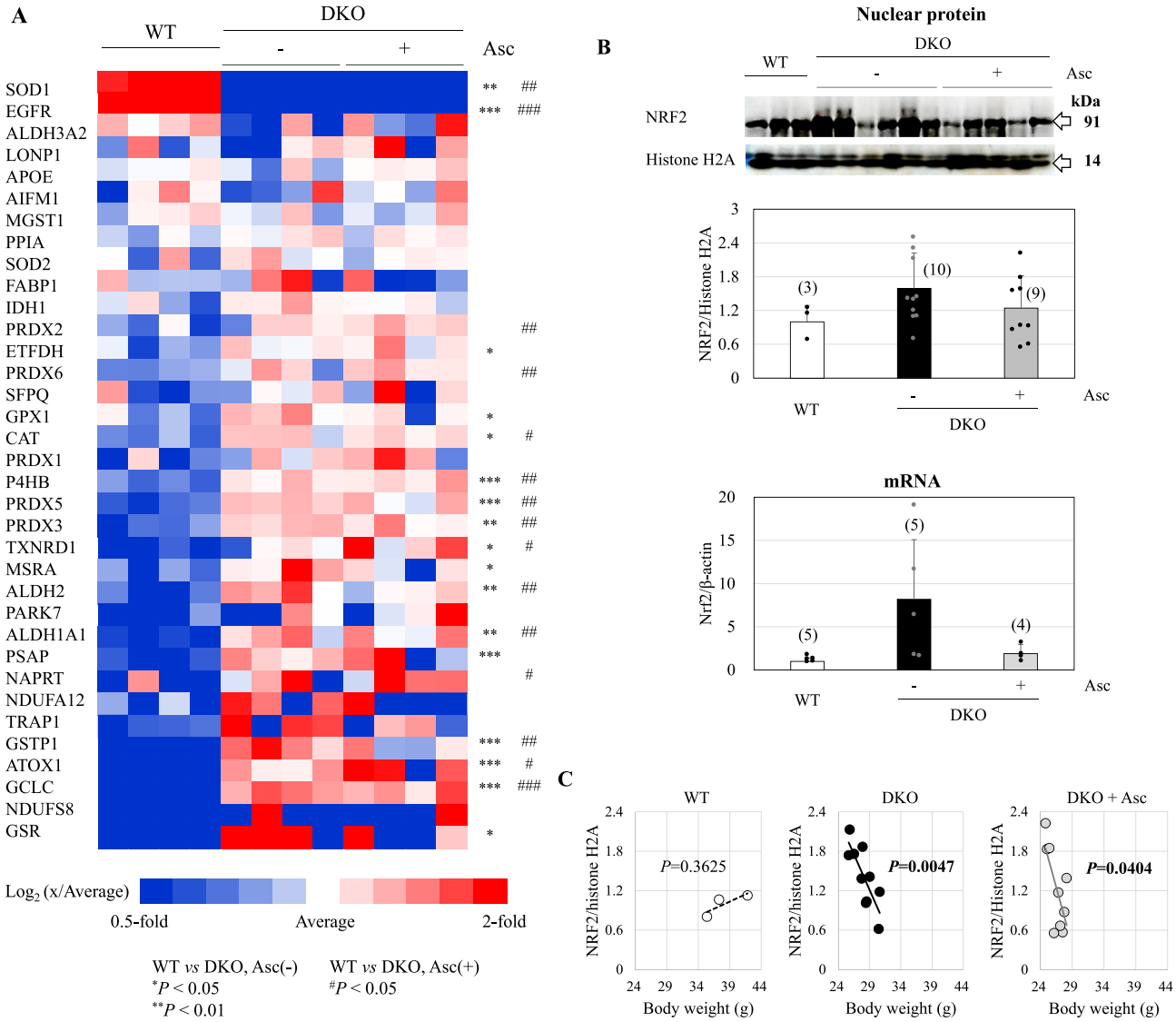

Fig. 5. Upregulation of antioxidant proteins and alterations in NRF2 in the liver of 8-month-old mice. (**A**) Heat map of antioxidant proteins (GO: 0,006,979, response to oxidative stress; 35/412 proteins) among three groups of mice. Statistical analyses were performed by Student's *t*-test. WT *vs* DKO mice: $^{*}P<0.05$, $^{**}P<0.01$, $^{***}P<0.001$. WT *vs* DKO + Asc: $^{\#}P<0.05$, $^{\#\#}P<0.01$, $^{\#\#\#}P<0.001$. (**B**) Immunoblot analysis of liver nuclear proteins with anti-NRF2 antibody (top). Signal intensity was quantified relative to histone H2A (middle). Nrf2 mRNA expression was measured by quantitative PCR relative to β-actin mRNA (bottom). Numbers in parentheses indicate the number of animals. Statistical analysis was performed using one-way ANOVA followed by the Tukey–Kramer test. (**C**) Correlation between NRF2 abundance (relative to histone H2A) and body weight in each group.

ACO1, but not ACO2, was decreased in DKO mice irrespective of Asc status (Fig. 6A). Consistently, aconitase activity, an intrinsic property of both ACO1 and ACO2, was reduced by approximately 50% in DKO mice, again regardless of Asc status (Fig. 6B), whereas no change was observed in free-iron content (Fig. 6C). The unchanged levels of citrate/isocitrate and the reduced levels of itaconic acid collectively suggest that the TCA cycle dependent on ACO2 activity is maintained in DKO mice. Taken together, these findings indicate that iron metabolism regulated by ACO1 is impaired in DKO mice.

Discussion

A novel finding of this study is that supplementation of DKO mice with physiological levels of Asc did not prevent NASH-mediated promotion to a precancerous state, but significantly suppressed progression to liver tumors (Figs. 1 and 2). Antioxidation is a well-established function of Asc[22], and improved survival of DKO mice could be attributed to the ability to eliminate ROS. Long-term exposure to stress conditions likely causes cell death and compensatory proliferation, which increases the risk of tumorigenic transformation via mutation[33]. Increased amino acid metabolism supports the aberrant proliferation of hepatic cells in DKO mice. In addition

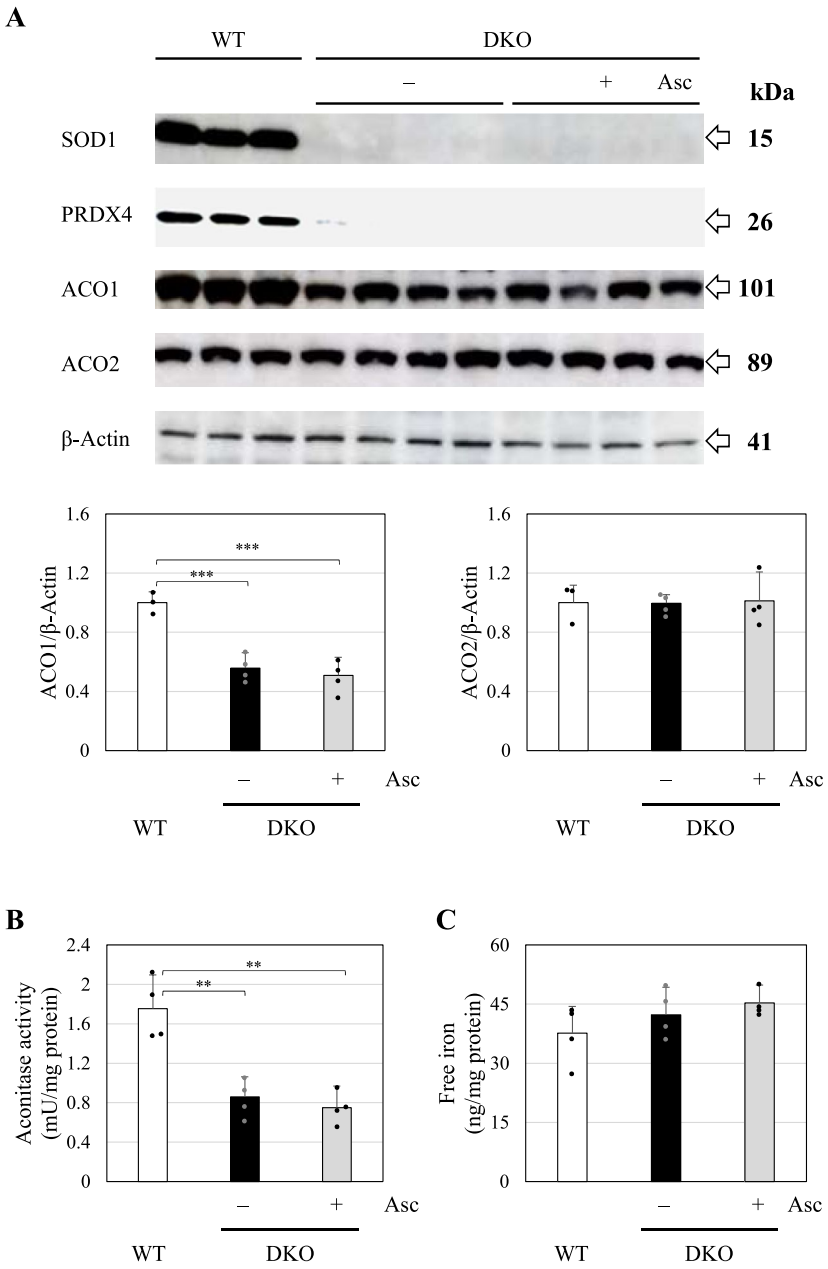

Fig. 6. Changes in the status of ACOs and iron. (**A**) Immunoblot analysis was performed on liver proteins using an antibody against SOD1, PRDX4, ACO1, and ACO2 and β-ACTIN. The signal intensity was quantified using ImageJ software and is expressed relative to the β-ACTIN band. $^{***}P<0.001$. (**B**) Aconitase activity was determined using a commercial assay kit without a further addition of iron. $^{**}P<0.01$. (**C**) Iron contents were determined using an iron assay kit; $n=4$ each in all experiments. Statistical analysis was performed using one-way ANOVA followed by the Tukey–Kramer test.

to its antioxidant activity, Asc can paradoxically promote ROS production in the presence of free iron[22]. Tumor cells are known to exhibit aberrant iron metabolism and contain higher levels of free iron compared with normal cells[31]. Given the presence of supplemented Asc and elevated free iron, the resultant ROS tend to cause ferroptosis in tumor-prone cells, thereby suppressing tumor development in Asc-supplemented DKO mice. Thus, the dual effects of Asc—protecting cells from oxidative damage and inducing ferroptosis in precancerous cells—appear to cooperate to enhance survival and suppress tumors in DKO mice.

The antitumor effects of Asc have been debated since the original proposal by Linus Pauling[34,35]. Recent studies suggest that pharmacologically high doses of Asc can exert therapeutic effects on advanced tumors[35–37], likely through ROS generation via Asc redox reactions catalyzed by free iron[36,38] and/or glutathione-dependent pathways[35]. Here, we found that administration of physiological doses of Asc, rather than pharmacologically high doses, could be beneficial in preventing hepatic tumor development. As a potent electron donor, Asc may

directly eliminate radical species and alleviate ER stress, thereby contributing to the survival of young mice through the normalization of cellular functions[22,39].

To our surprise, oxidative protein damage, as judged by carbonyl content, was decreased rather than increased in DKO mice. This unusual phenomenon could be partially explained by the stimulation of polyubiquitination of oxidized proteins and their subsequent degradation via the proteasome. ACO1 protein was among those decreased in DKO mice, potentially due to disruption of iron-sulfur clusters via increased ROS[29,40], which may perturb iron homeostasis in some precancerous cells, particularly those undergoing tumorigenic transformation. This effect is likely limited to a small fraction of precancerous cells at a given time, so the resulting free iron would have minimal impact on total hepatic levels. Nevertheless, at the single-cell level, redox recycling of free iron in the presence of Asc could promote hydroxyl radical production, leading to lipid peroxidation[22] and ferroptosis[30].

We identified eight proteins significantly decreased by Asc supplementation, several of which are involved in metabolic regulation and stress responses. Their reduction suggests that Asc may modulates oxidative stress and indirectly suppress aberrant cell proliferation via metabolic pathways. Further studies will be required to determine whether these proteins contribute to the observed suppression of tumorigenesis in DKO mice.

PRDX4 protects against inflammatory diseases such as dextran sulfate sodium-induced colitis by suppressing ER stress[41], and SOD1 protects against inflammation by reducing ROS-induced oxidative stress and pro-inflammatory responses[42]. Accordingly, the progression of inflammatory disease may be promoted in DKO mice. In these mice, nuclear NRF2 levels negatively correlated with body weight (Fig. 5B), and previous colitis models in *Prdx4*-KO or *Sod1*-KO mice showed greater weight loss and inflammation than WT mice, suggesting that higher oxidative stress induces more severe inflammation and hepatocyte death.

ROS can cause disease via cellular dysfunction and death, and in severe cases, ER stress can trigger cell-death pathways[43]. PRDX4 deficiency slightly increases hepatic tumor development, which is markedly enhanced by *N*-nitrosodiethylamine treatment[20]. ROS are abundantly produced during xenobiotic detoxification via cytochrome P450/reductase system[44], so combined oxidative and ER stress promotes tumorigenesis in *Prdx4*-KO mice. Similarly, Asc deficiency increases lethality and tumor development after *N*-nitrosodiethylamine exposure. In DKO mice, SOD1 deficiency increases ROS while decreasing Asc levels, with concomitant ER stress due to PRDX4 deficiency. In NASH-mediated hepatocarcinogenesis, cell death typically precedes fibrosis, which in turn promotes the progression to liver cancer[12,25]. However, fibrotic changes were not observed in DKO livers, likely due to insufficient Asc as a cofactor for collagen synthesis[18] and impaired ER function affecting fibrotic protein excretion. Impaired fibrosis may weaken tissue architecture and contribute to premature death.

Stronger positivity for FerAb, an antibody that recognizes oxidized phospholipids, was observed in precancerous lesions compared with cancerous lesions in the same liver (Fig. 2). This finding suggests that lipid peroxidation and subsequent ferroptotic cell death are more common in precancerous cells destined for proliferation and tumorigenesis. Iron can influence heterochromatin organization indirectly through oxidative stress generated by the Fenton reaction and modulate global histone methylation patterns via iron-dependent epigenetic enzymes in tumor cells, which typically contain higher levels of labile iron than normal cells. DKO mice exhibited lower ACO1 levels than WT mice, which could increase free iron in cells undergoing tumorigenic transformation. However, no significant differences in free iron were detected between precancerous livers of DKO and WT mice at 8 months, likely due to averaging across a small number of tumorigenic cells.

In this study, FerAb staining demonstrated increased ferroptotic cell death in the livers of DKO mice, particularly in precancerous regions. However, Asc supplementation did not alter the distribution of ferroptotic cells, suggesting that its hepatoprotective effect is not primarily mediated through suppression of ferroptosis. GPX4 protein levels were comparable among groups, indicating that ferroptosis in this model might occur through GPX4-independent pathways. Although lipid peroxidation was evident, these findings suggest that multiple oxidative stress–related mechanisms, beyond canonical ferroptosis, may contribute to liver injury and tumorigenesis in DKO mice. Further studies will be required to clarify these mechanisms.

A limitation of this study is that several mechanistic interpretations were inferred indirectly. For example, ER stress and NRF2 activation were assessed via downstream markers rather than direct functional assays, and protein oxidation, as indicated by carbonyl and polyubiquitin levels, is suggestive but not definitive of oxidative stress. In addition, the relatively small sample size may limit the detection of subtle differences in precancerous lesions. Further studies using larger cohorts and direct mechanistic approaches are needed to validate the pathways underlying Asc-mediated tumor suppression.

Because Asc has diverse functions, other mechanisms could also contribute to its antitumor effect. For instance, Asc-dependent prolyl hydroxylation can suppress HIF1α, a master regulator of the hypoxia pathway[45,46], and Asc-dependent TET-mediated DNA demethylation could epigenetically activate tumor-suppressor genes[47,48]. Further research is needed to understand the full range of Asc-mediated cancer-suppressing effects. DKO mice in this study developed cancer from NASH without fibrosis, which may differ from human hepatocarcinogenesis, but physiological Asc doses still inhibited tumor formation, potentially reducing side effects in clinical applications.

In summary, combined *Sod1* and *Prdx4* deficiency promotes liver tumor development, and Asc supplementation robustly suppresses this process. Asc acts as an antioxidant to reduce oxidative stress due to SOD1 deficiency, while also potentially inducing ferroptosis in precancerous lesions in the presence of iron ions. These results suggests that adequate Asc intake may prevent progression of fatty liver diseases under stressful conditions.

Materials and methods

Mice

Prdx4-KO mice were originally established in our institution. *Sod1*-KO mice were purchased from Jackson Laboratories (Bar Harbor, ME, USA). These mice were backcrossed to the C57BL/6N background for more than 10 generations. Establishment and breeding of the DKO mice were described in our previous study[21]. All mice

were weaned at 30 days of age and fed a standard diet (PicoLab 5053; LabDiet, St Louis, MO, USA) ad libitum with free access to water. Drinking water for additional groups of DKO and *Sod1*-KO mice was supplemented with Asc (1.5 mg/mL), as described previously[49]. The animal room was maintained under specific pathogen-free conditions at a constant temperature of 20–22 °C with a 12 h light/dark cycle.

Mice were euthanized by cervical dislocation without prior anesthesia, in accordance with the Yamagata University Animal Experimentation Guidelines and the protocol approved by the Animal Experimentation Committee (approval number: R6069). The procedure was performed by trained personnel. The body weight at the time of sacrifice was as follows: for 4-month-old mice, WT: 23.4–27.9 g (median 26.4 g), DKO: 27.4–28.9 g (median 28.1 g), and DKO supplemented with Asc: 20.2–27.7 g (median 24.9 g); for 8-month-old mice, WT: 33.1–41.8 g (median 37.3 g), DKO: 25.7–31.9 g (median 28.5 g), and DKO supplemented with Asc: 26.1–29.9 g (median 27.6 g).

Animal experiments were performed in accordance with institutional guidelines for the care and use of laboratory animals, as approved by the Animal Research Committee of Yamagata University (R6069). All methods are reported in full compliance with the ARRIVE guidelines.

Histological analyses of livers

Livers were harvested immediately after euthanization, immersed in 10% formalin, and fixed for 3 days at room temperature. Thereafter, the formalin was replaced with 70% ethanol, and the samples were stored in 70% ethanol at room temperature until paraffin embedding. The Sects. (5 μm thick) were stained with hematoxylin and eosin. Immunostaining was performed using the Leica Bond Max automated system (Leica, Bannockburn, IL, USA) with the Bond Intense R Detection Kit (DS9263). Antigen retrieval was carried out by immersion in BOND Epitope Retrieval Solution 1 (AR9961) for 10 min. FerAb[26] was diluted to 2 μg/mL in BOND Primary Antibody Diluent (AR9352). Biotin-conjugated goat anti-rat IgG (H + L) antibody (1:500) was used as the secondary antibody. Tissues were counterstained with hematoxylin, and microphotographs were acquired using a BX53 microscope and DP22 digital camera (Olympus, Tokyo, Japan).

Measurement of the reduced form of Asc

A fluorescent probe, 15-(Naphthalen-1-ylamino)-7-aza-3, 11-dioxadispiro [5.1.58.36] hexadecan-7-oxyl, was synthesized and used to measure the Asc, as described in the literature[50]. The Asc concentration was calculated by measuring the fluorescence at an excitation wavelength of 310 nm and an emission wavelength of 430 nm using a microplate reader (Varioskan Flash, Thermo Fisher Scientific, Waltham, MA, USA).

Preparation of plasma and liver lysate

Blood was collected from the tail vein into tubes containing ethylenediaminetetraacetic acid and centrifuged at 2,400 × *g* for 5 min, after which the plasma fraction was collected for analysis. Liver tissues dissected from mice were homogenized on ice in lysis buffer (25 mM Tris–HCl, pH 7.5, containing 150 mM NaCl, 1% NP-40, 1% sodium deoxycholate, and 0.1% SDS) supplemented with a protease inhibitor cocktail (P8340; Sigma-Aldrich, St. Louis, MO, USA), using a glass-Teflon homogenizer. The homogenates were centrifuged at 17,400 × *g* for 20 min at 4 °C. Protein concentrations in the supernatants were determined using the Pierce™ BCA protein Assay Kit (Thermo Fisher Scientific).

Proteomic analysis

Liver lysate samples (50 μg) were reduced using dithiothreitol (10 mM) followed by alkylation with iodoacetamide (25 mM). Following hydrolysis with trypsin, reaction mixtures were desalted using a C-Tip (Nikkyo Technos, Tokyo, Japan), as previously described in the literature[51]. The desalted peptide solution was analyzed via nanoflow liquid chromatography tandem mass spectrometry using an Easy nLC 1000 system (Thermo Fisher Scientific) connected to a hybrid quadrupole-Orbitrap mass spectrometer (Q-Exactive; Thermo Fisher Scientific) equipped with a nanoelectrospray emitter. The measurement conditions were previously described in the literature[52].

Raw file reads were matched against the Swiss-Prot house mouse database (17,162 sequences), using a Proteome Discoverer (version 1.4; Thermo Fisher Scientific) with the Sequest^{HT} and Mascot (version 2.8.0.1; Matrix Science, Tokyo, Japan) search engines. Precursor and fragment mass tolerances were set to 10 ppm and 0.04 Da, respectively. A fixed modification for *S*-carbamidomethylated cysteine and two maximum missed cleavage sites for trypsin were established. The results were filtered using a Percolator with a false discovery rate of 1%. The peak area of each identified peptide was estimated using a Proteome Discoverer. The intensity of unique peptides was used to calculate the protein intensity. An intensity-based absolute quantification algorithm was used to calculate the protein quantification values[53].

Metabolite analysis

Sample preparation and metabolite measurements were performed as described in the literature[54] with minor modifications. Alkylation was performed by treatment with 20 mM *N*-ethylmaleimide in 50 mM ammonium bicarbonate. Equal volumes of methanol containing both 10 μM of *N*-methylmaleimide-derivatized glutathione and 10 μM of L-methionine sulfone were added as internal standards. Following the addition of an equal volume of chloroform, the mixture was centrifuged at 12,000 × *g* for 15 min at 4 °C. The upper aqueous layer was lyophilized, dissolved in one-third volume of deionized water, and analyzed by liquid chromatography tandem mass spectrometry. A Q-Exactive hybrid quadrupole-Orbitrap mass spectrometer (Thermo Fisher Scientific) equipped with a heated electrospray ionization source was operated in the positive and negative ionization modes. The Ultimate 3000 LC system consisted of a WPS-3000 TRS autosampler, a TCC-3000 RS column oven, and an HPG-3400RS quaternary pump (Dionex, Sunnyvale, CA, USA). A SeQuant ZIC-pHILIC column (2.1 × 150 mm, 5 μm particle size; Merck KGaA, Darmstadt, Germany) and an Acquity UPLC BEH Amide

column (2.1 × 100 mm, 1.7 μm particle size; Waters Corp., Milford, MA, USA) were used to quantify as many metabolites as possible. For the ZIC-pHILIC column, the mobile phase A contained 20 mM of ammonium bicarbonate at pH 9.8, and the mobile phase B was 100% acetonitrile. For the BEH Amide column, mobile phase A was 0.1% formic acid and mobile phase B was 99.9% acetonitrile and 0.1% formic acid. System control and data acquisition were performed using Xcalibur 2.2 software.

All raw data collected were imported into Compound Discoverer 2.1 software (Thermo Fisher Scientific) for compositional determination. Elemental composition was searched using Compound Discoverer 2.1 against the mzVault metabolite database that was built in February 2017 based on accurate mass and isotopic patterns. Tentative metabolite identification was performed by comparing the observed full MS ions and MS/MS fragment ions, and validated identification was performed using reference standards. Compounds were grouped with a mass tolerance of 20 ppm and a retention time tolerance of 1 min and quantified based on the relative ameliorated peak area of each signal in the mass spectrum.

Protein data annotation

GO analysis of the differentially expressed genes was performed using the protein analysis through evolutionary relationships, and was adjusted for multiple testing via Bonferroni correction (GO database Released 2023–11-15). The *P*-value of each GO term above 0.05 was excluded from the analysis. The number of differentially expressed genes for particular GO terms was compared with the total number of genes assigned to each term, and enriched GO terms were presented. Differentially expressed genes were categorized as biological processes.

Preparation of nuclear fractions to detect NRF2

Liver tissues excised from mice were manually homogenized in 9 *vol.* of 0.25 M sucrose containing 3.3 mM of $CaCl_2$ and 5 mM of $MgCl_2$ using a glass-Teflon homogenizer on ice and subjected to centrifugation at 600 × *g* for 10 min. After washing twice with the same buffer, the pellets (nuclear fraction) were resuspended in 0.34 M of sucrose. Protein concentration was measured using a Pierce® BCA™ protein assay kit. The abundance of the nuclear fractionation was confirmed by immunoblotting using anti-histone H2A.x (3522–1; Epitmics, California, USA) as a nuclear protein marker.

Immunoblotting

Proteins in liver lysates (20–30 μg) were separated by SDS–polyacrylamide gel electrophoresis and blotted onto polyvinylidene difluoride membranes. The blots were blocked with 5% skim milk in tris-buffered saline containing 0.1% Tween-20, and were then incubated with the antibodies. The primary antibodies used were: GPX4 (ab125066; Abcam), SOD1[21], ACO1 (12,406–1-AP; Proteintech Group Inc.), ACO2 (67,509–1-IG; Proteintech Group Inc.), PRDX4[21], NRF2 (16,396–1-AP; Proteintech Group Inc.), histone H2A.x, 20Sα (BML-PW8195; Enzo Life Sciences), β1 (BML-PW8140; Enzo Life Sciences), β2 (BML-PW9300; Enzo Life Sciences), β5 (BML-PW8895; Enzo Life Sciences), and β-actin (sc-69879; Santa Cruz Biotechnology, Dallas, TX, USA). Either horseradish peroxidase-conjugated goat anti-rabbit IgG (sc-2357, Santa Cruz Biotechnology) or anti-mouse IgG (sc-2005, Santa Cruz Biotechnology) antibodies were used as the secondary antibodies. After washing, immune reactive bands were detected by measuring the chemiluminescence using an Immobilon western chemiluminescent HRP substrate (EMD Millipore, Temecula, CA, USA) on an image analyzer (ImageQuant LAS500; GE Healthcare, Buckinghamshire, UK).

Measurement of aconitase activity

Aconitase activity was measured via a coupled enzyme reaction in which citrate is converted to isocitrate using an aconitase activity assay kit (MAK051, Sigma-Aldrich) according to the manufacturer's instructions. Briefly, liver tissues were homogenized in an ice-cold assay buffer using a glass-Teflon homogenizer and centrifuged at 800 × *g* for 10 min at 4 °C. Samples were diluted twofold in assay buffer, and 50 μL samples were transferred to 96-well microplates. Reaction mixtures containing an enzyme mix and the substrate (50 μL) were mixed with each sample and incubated at 25 °C for 45 min. Developer (10 μL) was added to each well, mixed, and incubated at 25 °C for 10 min. The absorbance at 450 nm was measured and the amounts of isocitrate generated were calculated from a standard curve. The activities were corrected according to total protein content.

Reverse transcription (RT)-PCR and quantitative RT-PCR analyses of the produced DNA

RNA from mouse livers was purified using ISOGEN II (Nippon Gene, Tokyo, Japan), and cDNA was prepared using a Prime Script cDNA synthesis kit (TaKaRa, Kyoto, Japan). The cDNAs were amplified using the corresponding primers (Supplementary Table 3) followed by separation on agarose gels. Quantitative RT-PCR analyses were performed using the Step One real-time PCR system (Applied Biosystems, Tokyo, Japan) and the Thunderbird SYBR qPCR mix (TOYOBO, Osaka, Japan) according to the manufacturer's recommendations.

Measurement of free iron in the liver homogenate

Free-iron concentrations in the liver were determined by observing visible coloration due to the formation of a chelate complex between ferrozine and iron using an iron assay kit (Metallo assay; Metallogenics Co., Ltd., Chiba, Japan) according to the manufacturer's instructions. Briefly, the lung lysate was adjusted to pH 2–3 by adding hydrochloric acid, with centrifugation at 15,000 rpm for 15 min, and then the supernatant was collected. Iron concentration in the supernatant was determined by measuring the iron-ferrozine complex at a wavelength of 562 nm. Liver iron concentrations were corrected for total protein content.

Statistical analysis

Statistical analyses were conducted using JMP software, version 12.2.0 (SAS Institute, Cary, NC, USA). Data are presented as the mean ± standard error from at least three independent samples. Survival curves of DKO mice with or without Asc supplementation were generated using the Kaplan–Meier method and compared by the log-rank test. Tumor incidence rates were analyzed with the chi-square test. Comparisons between two groups were performed using Student's *t*-test, whereas comparisons among multiple groups were assessed by one-way analysis of variance (ANOVA) followed by the Tukey–Kramer test. PCA was conducted using 20 glycometabolites (Fig. 4C) and 24 amino acid metabolites (Fig. 4D). A P-value < 0.05 was considered statistically significant.

Data availability

The raw data and analysis files have been deposited to the ProteomeXchange Consortium *via* the jPOST partner repository[55]with the data set identifier PXD058371 (JPST003491).

Received: 13 August 2025; Accepted: 13 November 2025
Published online: 22 December 2025

References

1. Goh, G. B. & McCullough, A. J. Natural history of nonalcoholic fatty liver disease. *Dig. Dis. Sci.* **61**, 1226–1233. https://doi.org/10.1007/s10620-016-4095-4 (2016).
2. Ioannou, G. N. Epidemiology and risk-stratification of NAFLD-associated HCC. *J. Hepatol.* **75**, 1476–1484. https://doi.org/10.1016/j.jhep.2021.08.012 (2021).
3. Shen, X., Yu, Z., Wei, C., Hu, C. & Chen, J. Iron metabolism and ferroptosis in nonalcoholic fatty liver disease: What is our next step?. *Am. J. Physiol. Endocrinol. Metab.* **326**, E767–E775. https://doi.org/10.1152/ajpendo.00260.2023 (2024).
4. Marengo, A., Rosso, C. & Bugianesi, E. Liver cancer: Connections with obesity, fatty liver, and cirrhosis. *Annu. Rev. Med.* **67**, 103–117. https://doi.org/10.1146/annurev-med-090514-013832 (2016).
5. Kohlhepp, M. S., Liu, H., Tacke, F. & Guillot, A. The contradictory roles of macrophages in non-alcoholic fatty liver disease and primary liver cancer-Challenges and opportunities. *Front. Mol. Biosci.* **10**, 1129831. https://doi.org/10.3389/fmolb.2023.1129831 (2023).
6. Chen, Z., Tian, R., She, Z., Cai, J. & Li, H. Role of oxidative stress in the pathogenesis of nonalcoholic fatty liver disease. *Free Radic. Biol. Med.* **15**, 116–141. https://doi.org/10.1016/j.freeradbiomed.2020.02.025 (2020).
7. Sutti, S. & Albano, E. Adaptive immunity: An emerging player in the progression of NAFLD. *Nat. Rev. Gastroenterol. Hepatol.* **17**, 81–92. https://doi.org/10.1038/s41575-019-0210-2 (2020).
8. Fridovich, I. Superoxide radical and superoxide dismutases. *Annu. Rev. Biochem.* **64**, 97–112. https://doi.org/10.1146/annurev.bi.64.070195.000525 (1995).
9. Uchiyama, S., Shimizu, T. & Shirasawa, T. CuZn-SOD deficiency causes ApoB degradation and induces hepatic lipid accumulation by impaired lipoprotein secretion in mice. *J. Biol. Chem.* **281**, 31713–31719. https://doi.org/10.1074/jbc.M603422200 (2006).
10. Elchuri, S. et al. CuZn-SOD deficiency leads to persistent and widespread oxidative damage and hepatocarcinogenesis later in life. *Oncogene* **24**, 367–380. https://doi.org/10.1038/sj.onc.1208207 (2005).
11. Erker, L. et al. Effect of the reduction of superoxide dismutase 1 and 2 or treatment with alpha-tocopherol on tumorigenesis in Atm-deficient mice. *Free Radic. Biol. Med.* **41**, 590–600. https://doi.org/10.1016/j.freeradbiomed.2006.04.032 (2006).
12. Wang, M. & Kaufman, R. J. The impact of the endoplasmic reticulum protein-folding environment on cancer development. *Nat. Rev. Cancer* **14**, 581–597. https://doi.org/10.1038/nrc3800 (2014).
13. Luna-Marco, C., Ubink, A., Kopsida, M. & Heindryckx, F. Endoplasmic reticulum stress and metabolism in hepatocellular carcinoma. *Am. J. Pathol.* **193**, 1377–1388. https://doi.org/10.1016/j.ajpath.2022.09.012 (2023).
14. Sekiya, M., Hiraishi, A., Touyama, M. & Sakamoto, K. Oxidative stress induced lipid accumulation *via* SREBP1c activation in HepG2 cells. *Biochem. Biophys. Res. Commun.* **375**, 602–607. https://doi.org/10.1016/j.bbrc.2008.08.068 (2008).
15. Sato, Y. et al. Synergistic cooperation of PDI family members in peroxiredoxin 4-driven oxidative protein folding. *Sci. Rep.* **3**, 2456. https://doi.org/10.1038/srep02456 (2013).
16. Fujii, J., Ochi, H. & Yamada, S. A comprehensive review of peroxiredoxin 4, a redox protein evolved in oxidative protein folding coupled with hydrogen peroxide detoxification. *Free Radic. Biol. Med.* **227**, 336–354. https://doi.org/10.1016/j.freeradbiomed.2024.12.015 (2024).
17. Zito, E., Chin, K. T., Blais, J., Harding, H. P. & Ron, D. ERO1-beta, a pancreas-specific disulfide oxidase, promotes insulin biogenesis and glucose homeostasis. *J. Cell Biol.* **188**, 821–832. https://doi.org/10.1083/jcb.200911086 (2010).
18. Zito, E., Hansen, H. G., Yeo, G. S., Fujii, J. & Ron, D. Endoplasmic reticulum thiol oxidase deficiency leads to ascorbic acid depletion and noncanonical scurvy in mice. *Mol. Cell* **48**, 39–51. https://doi.org/10.1016/j.molcel.2012.08.010 (2012).
19. Nabeshima, A. et al. Peroxiredoxin 4 protects against nonalcoholic steatohepatitis and type 2 diabetes in a nongenetic mouse model. *Antioxid. Redox Signal.* **19**, 1983–1998. https://doi.org/10.1089/ars.2012.4946 (2013).
20. Guo, X. et al. The association of peroxiredoxin 4 with the initiation and progression of hepatocellular carcinoma. *Antioxid. Redox Signal.* **30**, 1271–1284. https://doi.org/10.1089/ars.2017.7426 (2019).
21. Homma, T. et al. Double knockout of peroxiredoxin 4 (*Prdx4*) and superoxide dismutase 1 (*Sod1*) in mice results in severe liver failure. *Oxid. Med. Cell. Longev.* **2018**, 2812904. https://doi.org/10.1155/2018/2812904 (2018).
22. Njus, D., Kelley, P. M., Tu, Y. J. & Schlegel, H. B. Ascorbic acid: The chemistry underlying its antioxidant properties. *Free Radic. Biol. Med.* **159**, 37–43. https://doi.org/10.1016/j.freeradbiomed.2020.07.013 (2020).
23. Sentman, M. L. et al. Phenotypes of mice lacking extracellular superoxide dismutase and copper- and zinc-containing superoxide dismutase. *J. Biol. Chem.* **281**, 6904–6909. https://doi.org/10.1074/jbc.M510764200 (2006).
24. Iuchi, Y. et al. Elevated oxidative stress in erythrocytes due to a SOD1 deficiency causes anaemia and triggers autoantibody production. *Biochem. J.* **402**, 219–227. https://doi.org/10.1042/BJ20061386 (2007).
25. Horn, P. & Tacke, F. Metabolic reprogramming in liver fibrosis. *Cell Metab.* **36**, 1439–1455. https://doi.org/10.1016/j.cmet.2024.05.003 (2024).
26. Kobayashi, S., Harada, Y., Homma, T., Yokoyama, C. & Fujii, J. Characterization of a rat monoclonal antibody raised against ferroptotic cells. *J. Immunol. Methods* **489**, 112912. https://doi.org/10.1016/j.jim.2020.112912 (2021).
27. Yamamoto, M., Kensler, T. W. & Motohashi, H. The Keap1-Nrf2 system: A thiol-based sensor-effector apparatus for maintaining redox homeostasis. *Physiol. Rev.* **98**, 1169–1203. https://doi.org/10.1152/physrev.00023.2017 (2018).
28. Davies, K. J. Protein damage and degradation by oxygen radicals. *I. general aspects. J. Biol. Chem.* **262**, 9895–9901 (1987).
29. Demasi, M. et al. Redox regulation of the proteasome *via* *S*-glutathionylation. *Redox Biol.* **2**, 44–51. https://doi.org/10.1016/j.redox.2013.12.003 (2013).
30. Stockwell, B. R. Ferroptosis turns 10: Emerging mechanisms, physiological functions, and therapeutic applications. *Cell* **185**, 2401–2421. https://doi.org/10.1016/j.cell.2022.06.003 (2022).

31. Motooka, Y. & Toyokuni, S. Ferroptosis as ultimate target of cancer therapy. *Antioxid. Redox Signal.* **39**, 206–223. https://doi.org/10.1089/ars.2022.0048 (2023).
32. Rouault, T. A. The role of iron regulatory proteins in mammalian iron homeostasis and disease. *Nat. Chem. Biol.* **2**, 406–414. https://doi.org/10.1038/nchembio807 (2006).
33. Klaunig, J. E. & Kamendulis, L. M. The role of oxidative stress in carcinogenesis. *Annu. Rev. Pharmacol. Toxicol.* **44**, 239–267. https://doi.org/10.1146/annurev.pharmtox.44.101802.121851 (2004).
34. Cameron, E. & Pauling, L. Supplemental ascorbate in the supportive treatment of cancer: Prolongation of survival times in terminal human cancer. *Proc. Natl. Acad. Sci. USA* **73**, 3685–3689. https://doi.org/10.1073/pnas.73.10.3685 (1976).
35. Reczek, C. R. & Chandel, N. S. Cancer. *Revisiting vitamin C and cancer. Science* **350**, 1317–1318. https://doi.org/10.1126/science.aad8671 (2015).
36. Chen, Q. et al. Ascorbate in pharmacologic concentrations selectively generates ascorbate radical and hydrogen peroxide in extracellular fluid *in vivo*. *Proc. Natl. Acad. Sci. USA* **104**, 8749–8754. https://doi.org/10.1073/pnas.0702854104 (2007).
37. Villagran, M., Ferreira, J., Martorell, M. & Mardones, L. The role of vitamin C in cancer prevention and therapy: A literature review. *Antioxidants* **10**, 1894. https://doi.org/10.3390/antiox10121894 (2021).
38. Ghanem, A. et al. Ascorbate kills breast cancer cells by rewiring metabolism *via* redox imbalance and energy crisis. *Free Radic. Biol. Med.* **163**, 196–209. https://doi.org/10.1016/j.freeradbiomed.2020.12.012 (2021).
39. Pozzer, D., Invernizzi, R. W., Blaauw, B., Cantoni, O. & Zito, E. Ascorbic acid route to the endoplasmic reticulum: Function and role in disease. *Antioxid. Redox Signal.* **34**, 845–855. https://doi.org/10.1089/ars.2019.7912 (2021).
40. Castro, L., Tórtora, V., Mansilla, S. & Radi, R. Aconitases: Non-redox iron-sulfur proteins sensitive to reactive species. *Acc. Chem. Res.* **52**, 2609–2619. https://doi.org/10.1021/acs.accounts.9b00150 (2019).
41. Takagi, T. et al. Elevated ER stress exacerbates dextran sulfate sodium-induced colitis in PRDX4-knockout mice. *Free Radic. Biol. Med.* **134**, 153–164. https://doi.org/10.1016/j.freeradbiomed.2018.12.024 (2019).
42. Hwang, J. et al. SOD1 suppresses pro-inflammatory immune responses by protecting against oxidative stress in colitis. *Redox Biol.* **37**, 101760. https://doi.org/10.1016/j.redox.2020.101760 (2020).
43. Walter, P. & Ron, D. The unfolded protein response: from stress pathway to homeostatic regulation. *Science* **334**, 1081–1086. https://doi.org/10.1126/science.1209038 (2011).
44. Hrycay, E. G. & Bandiera, S. M. Involvement of cytochrome P450 in reactive oxygen species formation and cancer. *Adv. Pharmacol.* **74**, 35–84. https://doi.org/10.1016/bs.apha.2015.03.003 (2015).
45. McGettrick, A. F. & O'Neill, L. A. J. The role of HIF in immunity and inflammation. *Cell Metab.* **32**, 524–536. https://doi.org/10.1016/j.cmet.2020.08.002 (2020).
46. Kaelin, W. G. Jr. & Ratcliffe, P. J. Oxygen sensing by metazoans: The central role of the HIF hydroxylase pathway. *Mol. Cell* **30**, 393–402. https://doi.org/10.1016/j.molcel.2008.04.009 (2008).
47. Mikkelsen, S. U., Gillberg, L., Lykkesfeldt, J. & Grønbæk, K. The role of vitamin C in epigenetic cancer therapy. *Free Radic. Biol. Med.* **170**, 179–193. https://doi.org/10.1016/j.freeradbiomed.2021.03.017 (2021).
48. Berretta, M. et al. Multiple effects of ascorbic acid against chronic diseases: Updated evidence from preclinical and clinical studies. *Antioxidants* **9**, 1182. https://doi.org/10.3390/antiox9121182 (2020).
49. Homma, T. et al. Defective biosynthesis of ascorbic acid in *Sod1*-deficient mice results in lethal damage to lung tissue. *Free Radic. Biol. Med.* **162**, 255–265. https://doi.org/10.1016/j.freeradbiomed.2020.10.023 (2021).
50. Matsuoka, Y., Yamato, M., Yamasaki, T., Mito, F. & Yamada, K. Rapid and convenient detection of ascorbic acid using a fluorescent nitroxide switch. *Free Radic. Biol. Med.* **53**, 2112–2118. https://doi.org/10.1016/j.freeradbiomed.2012.09.032 (2012).
51. Osaki, T., Sugiyama, D., Magari, Y., Souri, M. & Ichinose, A. Rapid immunochromatographic test for detection of anti-factor XIII A subunit antibodies can diagnose 90 % of cases with autoimmune haemorrhaphilia XIII/13. *Thromb. Haemost.* **113**, 1347–1356. https://doi.org/10.1160/TH14-09-0745 (2015).
52. Homma, T., Fujiwara, H., Osaki, T., Fujii, S. & Fujii, J. Consequences of a peroxiredoxin 4 (*Prdx4*) deficiency on learning and memory in mice. *Biochem. Biophys. Res. Commun.* **621**, 32–38. https://doi.org/10.1016/j.bbrc.2022.06.096 (2022).
53. Schwanhäusser, B. et al. Global quantification of mammalian gene expression control. *Nature* **473**, 337–342. https://doi.org/10.1038/nature10098 (2011).
54. Kobayashi, S. et al. Carnosine dipeptidase II (CNDP2) protects cells under cysteine insufficiency by hydrolyzing glutathione-related peptides. *Free Radic. Biol. Med.* **174**, 12–27. https://doi.org/10.1016/j.freeradbiomed.2021.07.036 (2021).
55. Okuda, S. et al. jPOSTrepo: An international standard data repository for proteomes. *Nucleic Acids Res.* **45**, D1107–D1111. https://doi.org/10.1093/nar/gkw1080 (2017).

Acknowledgements

We thank the Support Group for Pathologic Analysis, a Grant-in-Aid for Scientific Research on Innovative Areas "Advanced Animal Model Support (AdAMS)" from the MEXT, Japan (KAKENHI 22H04922).

Author contributions

Conceptualization, J.F.; methodology, T.O., Y.M, and S.T.; formal analysis, T.O., Y.M, and S.T.; investigation, T.O., T.H., and Y.M.; resources, K.-I. Y. and C.Y.; writing, J.F.; funding acquisition, T.O., S.T. and J.F. All authors have read and agreed to the published version of the manuscript.

Funding

This research was funded by the JSPS KAKENHI (23K06410) to T.O., JSPS KAKENHI (24K10074) and Yamagata University the YU-COE program (S6) to J.F., JSPS KAKENHI (JP19H05462, JP20H05502) and JST CREST (JPMJCR19H4) to S.T.

Declarations

Competing interests

The authors declare no competing interests.

Additional information

Supplementary Information The online version contains supplementary material available at https://doi.org/10.1038/s41598-025-28982-8.

Correspondence and requests for materials should be addressed to T.O.